J. Meas. Sci. Instrum., 2026, 17(1): 133-140. http://jmsi.publish.founderss.cn/
DOI: 10.62756/jmsi.1674-8042.2026011 jmsi@nuc.edu.cn

Simulation and analysis of Ag/ZnO/AZO/Al photodetector

ZHANG Caizhen*, HU Tong, FANG Hengtong, SHEN Lingqin

School of Elecrtonics and Information Engineering, Lanzhou Jiaotong University, Lanzhou 730070, China

***Corresponding author:** ZHANG Caizhen (19871092116@163.com)

Received: May 28, 2025 **Revised:** July 3, 2025 **Accepted:** October 19, 2025

Abstract: The introduction of an aluminum-doped zinc oxide (AZO) buffer layer on a glass substrate has been shown to enhance the performance of Ag/ZnO Schottky photodetectors. To further investigate the correlation between the parameters of AZO buffer layer and ZnO active layer and the performance of Ag/ZnO/AZO/Al photodetectors, we constructed an Ag/ZnO/AZO/Al photodetector based on Silvaco TCAD simulation platform to investigate the effects of AZO layer thickness, ZnO layer thickness, AZO doping concentration, and ZnO doping concentration on the device performance. The simulation results demonstrate that the device achieves better performance when the AZO layer thickness ranges from 0.8 μm to 1.2 μm and the ZnO layer thickness ranges from 0.5 μm to 0.8 μm, with an AZO doping concentration of 1×10^{19} cm^{-3} and a ZnO doping concentration of 1×10^{16} cm^{-3}. Increasing the doping concentration of the AZO buffer layer can enhance the electric field intensity at ZnO-AZO interface, effectively preventing photogenerated holes from approaching ZnO-AZO interface so as to reduce interface recombination; while appropriate ZnO layer thickness and doping concentration can optimize the space charge region width and carrier collection efficiency. Under these optimized conditions, the photodetector reaches its optimum performance with a dark current of 1.1×10^{-8} A, a photocurrent of 8.41×10^{-6} A, and a responsivity of 0.21 $A\cdot W^{-1}$. This research helps reduce the number of experiments and associated costs while preparing low-cost and high-performance ZnO photodetectors.

Key words: aluminum-doped zinc oxide (AZO); zinc oxide (ZnO); Schottky; ultraviolet (UV) photodetector; electric field distribution; dark current

0 Introduction

Ultraviolet (UV) photodetectors have a wide range of applications in the fields of environmental monitoring, solar astronomical observation, biomedicine[1-3], etc. Zinc oxide (ZnO), as a wide-bandgap semiconductor material (bandwidth ~3.37 eV), is an ideal candidate for UV photodetectors owing to its high exciton binding energy (60 meV) and high UV absorption coefficient[4]. ZnO photodetectors can be classified into metal-semiconductor-metal(MSM), Schottky, heterojunction, p-i-n, etc[5-8]. Among them, Schottky photodetectors have attracted significant attention due to their advantages of low dark current, simple fabrication process, elimination of p-type doping requirements, and fast response speed[9-10].

Recognizing that Silvaco TCAD simulation software can significantly reduce experimental iterations, researchers have recently employed this platform to systematically analyze the effects of both material and structural parameters on the optoelectronic performance of UV photodetectors. Sharma et al.[4] conducted simulations on n-ZnO/p-Si heterojunction photodetectors, demonstrating that the responsivity increases with ZnO thickness but decreases with doping concentration, while maintaining a dark current on the order of 10^{-14} A. Singh[11] performed both simulations and experimental investigations on aluminum-doped zinc oxide (AZO)-based MSM photodetectors, revealing that the resistance increases with electrode spacing under both dark and UV illumination conditions, with a light-to-dark current ratio reaching 10^2. Al-Khalli et al.[12] examined the performance of ZnO-based thin-film MSM photodetectors fabricated on p-type Si substrates, achieving a responsivity of 0.043 $A\cdot W^{-1}$ and a dark current of 2.19×10^{-9} A at an optimal finger spacing of 1 μm and ZnO active layer thickness of 1 μm. However, most of these studies have focused on conventional silicon or sapphire substrates, with relatively few investigations addressing Schottky ZnO photodetectors on glass substrates. The significant lattice mismatch between glass substrate and ZnO film can induce elevated interface defect state densities, consequently leading to increased dark current and degraded photoelectric performance[13]. To

address this issue, Zhang et al.[14] successfully fabricated an Ag/ZnO/AZO/Al UV photodetector by introducing an AZO buffer layer on the glass substrate, effectively mitigating the impact of interface defects. Nevertheless, systematic studies on how the parameters of the AZO buffer layer and ZnO active layer influence the optoelectronic performance of such devices remain lacking.

In this study, by means of Silvaco TCAD simulation tools, we modeled the structure of an Ag/ZnO/AZO/Al photodetector and investigated the effects the thickness and doping concentration of the AZO buffer layer as well as the ZnO active layer on the detector performance. Simulation results are highly consistent with the experimental results, which means that our work can significantly reduce the number of experiments and associated costs while providing theoretical guidance for the development of high-performance Schottky photodetectors on the low-cost glass substrate.

1 Device structure and material parameters

The structure of the designed Ag/ZnO/AZO/Al photodetector is shown in Fig.1.

We simulated it on Silvaco-TCAD platform, and a partially enlarged simulation structure of the device is shown in Fig. 2. The simulation structure consists of a 300-μm thick boron-silicate glass (BSG) substrate, a 1.0-μm thick AZO buffer layer with the n-type doping concentration set to 1×10^{18} cm^{-3}, and a 0.5 μm thick ZnO layer from bottom to top[14]. The device width is set to 20 000 μm. The anode is an Al electrode with a thickness of 0.1 μm and a length of 1.0 μm, while the cathode is an Ag electrode with the thickness and length of 0.15 μm and 1.0 μm, respectively[14]. The Al electrode forms an ohmic contact with the AZO film, and the Ag electrode forms a Schottky contact with the ZnO film.

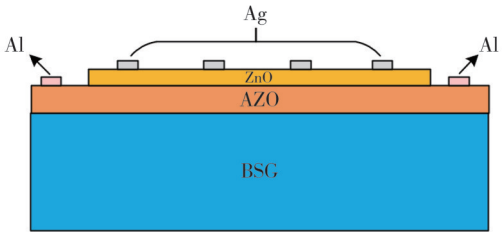

Fig. 1 Structure of Ag/ZnO/AZO/Al photodetector

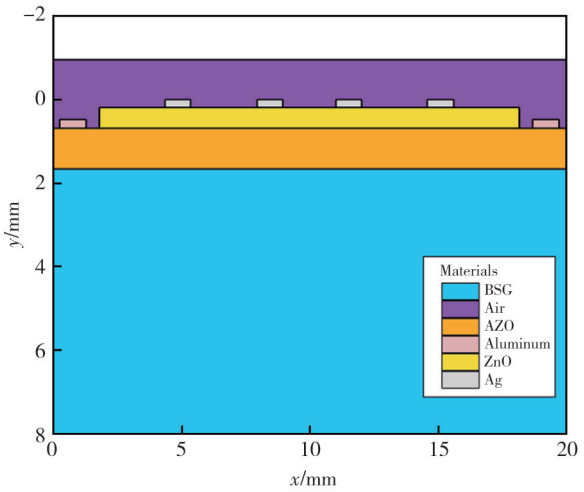

Fig. 2 Simulated structure of Ag/ZnO/AZO/Al photodetector by Silvaco-TCAO

Table 1 lists some of the material parameters used in the simulation[4,15-17].

Table 1 Some material parameters used in simulation

Material	Thickness/μm	Bandgap E_g/eV	Electron affinity χ/eV	Relative permittivity ε_r	Electron mobility μ_n/($cm^2 \cdot V^{-1} \cdot s^{-1}$)	Hole mobility μ_p/($cm^2 \cdot V^{-1} \cdot s^{-1}$)	Effective density of states in conduction band N_c/($\times10^{18}$ cm^{-3})	Effective density of states in valence band N_v/($\times10^{19}$ cm^{-3})
ZnO	0.5	3.35	4.2	9.4	270	70	2.2	1.8
AZO	1.0	3.04	4.4	9	270	70	2.2	1.8

The Shockley-Read-Hall recombination model (SRH), Auger recombination model (Auger), Fermi carrier statistical model (Fermi), concentration-dependent mobility model (Commob), and optical generation recombination model (Optr)[4,18] were used in the simulation.

Fig. 3 presents the simulated and experimental *I-V* characteristics of the Ag/ZnO/AZO/Al photodetector[15]. The results demonstrate good agreement between the simulated and experimental photocurrent/dark current, validating the reliability of the model and parameter settings. This provides theoretical support for further investigation into the relationship between the AZO buffer layer, ZnO active layer and device performance.

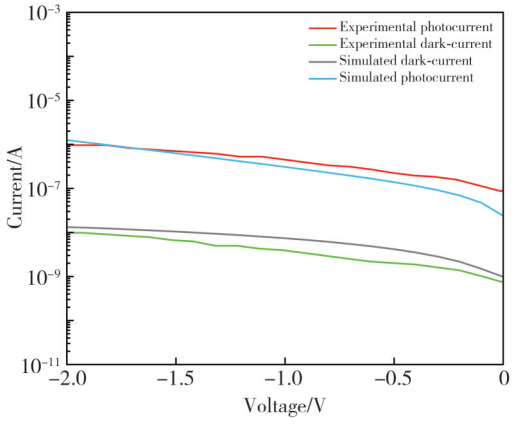

Fig. 3 Simulated and experimental *I-V* characteristics

2 Results and discussion

2.1 Effect of AZO layer thickness on device performance

To investigate the AZO thickness effect, we varied the layer thickness from 0.2 μm to 1.2 μm (in 0.2-μm increment) and analyzed the resulting variations in photocurrent, dark current, and responsivity.

Fig. 4 presents the *I-V* characteristics under different AZO layer thicknesses.

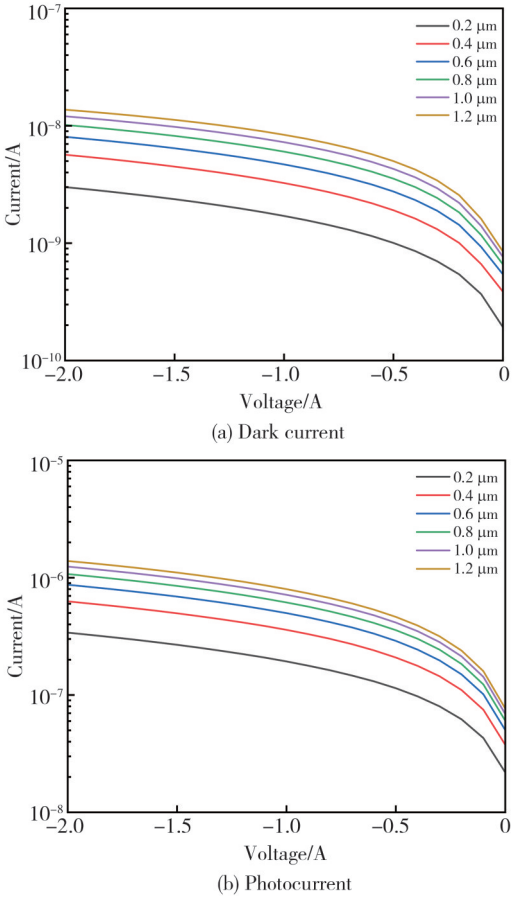

Fig. 4 *I-V* characteristics at different AZO layer thicknesses

Fig. 4(a) displays the dark current graph under different AZO layer thicknesses, which reveals a clear positive correlation between AZO thickness and dark current. When the AZO thickness reaches 1.2 μm, the dark current is the highest, about 1.37×10^{-8} A, while the dark current corresponding to the thinner AZO layer (e.g., 0.2 μm) is lower, about 3.0×10^{-9} A. Fig. 4(b) shows the photocurrent diagram for different AZO layer thicknesses. It can be observed that with the increase in AZO layer thickness, the photocurrent of the device gradually increases. At 1.2 μm thickness, the photocurrent reaches the highest, about 1.39×10^{-6} A, while the photocurrent corresponding to the thinner AZO layer (e.g., 0.2 μm) is lower, about 3.40×10^{-7} A. This trend likely stems from the thicker AZO layer that increases the carrier conduction path, thereby reducing the resistance of the AZO buffer layer, resulting in an increase in current, which is consistent with the research results of Novák et al.[19] on the correlation between AZO film thickness and resistivity.

Fig. 5 shows the responsivity at different AZO layer thicknesses. With the increase of AZO layer thickness, the responsivity of the device improves overall and reaches a peak value near 0.36 μm. Thinner AZO layers (e.g., 0.2 μm) have relatively lower responsivity, while appropriately increasing the AZO thickness (e. g., 0.6 μm and 0.8 μm) can effectively improve the responsivity of the device. However, when the AZO layer thickness continues to increase to 1.2 μm, the responsivity enhancement tends to saturate with little change. In summary, the most suitable range of AZO layer thickness is 0.8—1.2 μm, which is consistent with the conclusion of Ref.[20].

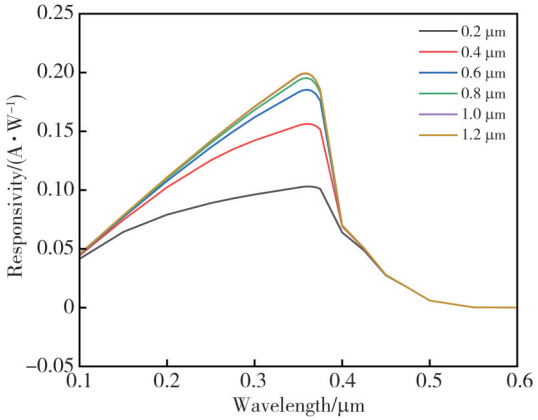

Fig. 5 Responsivity at different AZO layer thicknesses

2.2 Effect of ZnO layer thickness on device performance

To investigate the impact of ZnO layer thickness on device performance, we varied the thickness from 0.2 μm to 1.2 μm (0.2, 0.5, 0.8, 1.0, and 1.2 μm) and analyzed the resulting variations in photocurrent, dark current, electric field distribution, recombination rate, and responsivity.

Fig. 6 shows the *I-V* characteristics for different ZnO layer thicknesses. Fig. 6(a) presents the dark current plots at different ZnO layer thicknesses, and it can be seen that the dark current of the device decreases gradually with the increase of the ZnO layer thickness. When the thickness of ZnO layer is 0.2 μm, the dark current is the highest, about 1.32×10^{-8} A, and when the thickness of ZnO layer increases to 1.2 μm, the dark current decreases to 1.01×10^{-8} A. Fig. 6(b) shows the

photocurrent plots under different ZnO layer thicknesses. When the ZnO layer thickness increases from 0.2 μm to 1.0 μm, the photocurrent of the device increases, while the photocurrent decreases when the ZnO layer thickness is 1.2 μm.

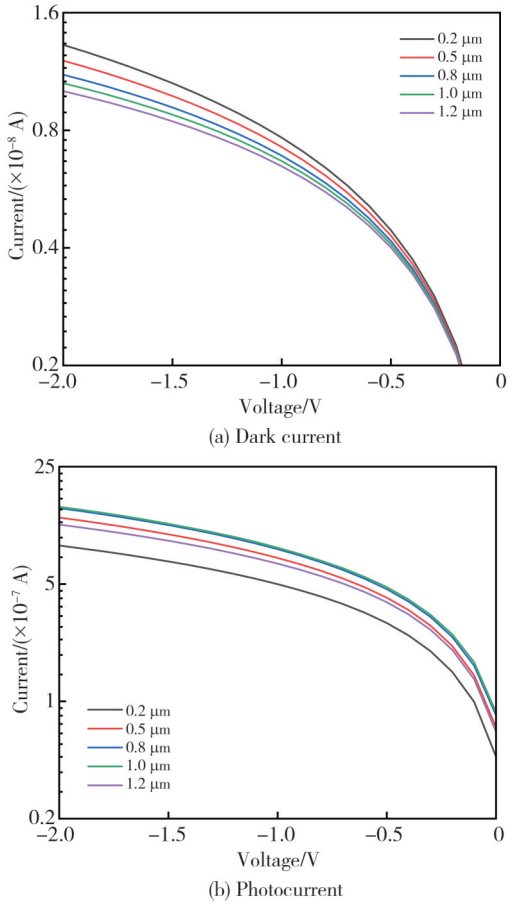

Fig. 6 *I-V* characteristics at different ZnO layer thicknesses

Fig. 7 shows the recombination rate and electric field distribution for different ZnO layer thicknesses. According to the recombination rate in Fig. 7(a), it can be seen that the recombination rate decreases as the ZnO thickness increases, which will lead to a decrease in the dark current and a larger photocurrent. As shown in Fig. 7(b), as the thickness of ZnO increases beyond 1.0 μm, the width of the space charge region does not expand correspondingly. This results in an increased length of the undepleted neutral region where carriers must traverse, leading to a reduction in carrier collection efficiency and consequently a decrease in photocurrent.

Fig.8 illustrates the responsivity at different ZnO layer thicknesses. It can be seen that the device exhibits weak responsivity with thin ZnO layers (e.g., 0.2 μm), but shows significant enhancement when the thickness increases to 0.5 μm. However, when the ZnO layer thickness further increases to 1.0 μm, the peak responsivity gradually starts to decrease. In summary, the most suitable range of ZnO layer thickness is 0.5—0.8 μm.

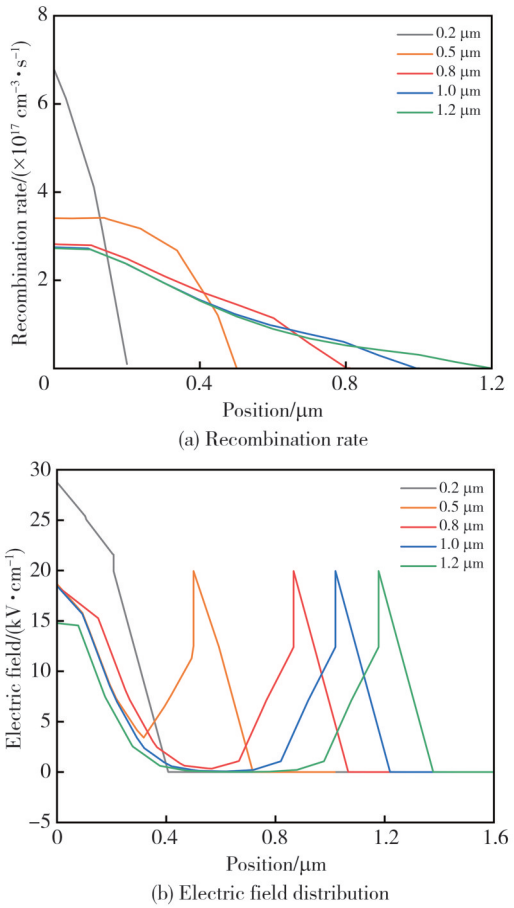

Fig. 7 Recombination rate and electric field distribution for different ZnO layer thicknesses

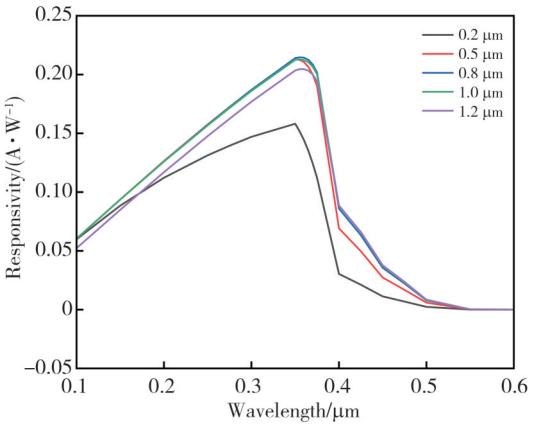

Fig. 8 Responsivity at different ZnO layer thicknesses

2.3 Effect of AZO layer doping concentration on device performance

To investigate the influence of AZO doping concentration on device performance, we varied the doping level from 1×10^{16} cm^{-3} to 1×10^{20} cm^{-3}, and analyzed the resulting variations in photocurrent, dark current, electric field distribution, and responsivity.

Fig. 9 shows the *I-V* characteristics of the AZO layer

at different doping concentrations. Fig.9(a) presents the dark current plots of the AZO layer under different doping concentrations. The dark current initially increases with doping concentration, however, when the concentration exceeds 1×10^{19} cm^{-3}, the dark current decreases. Fig.9(b) shows the photocurrent plots of the AZO layer at different doping concentrations, and it can be observed that the photocurrent gradually increases when the doping concentration ranges from 1×10^{16} cm^{-3} to 1×10^{18} cm^{-3}, and reaches its maximum when the doping concentration is 1×10^{19} cm^{-3}, whereas it decreases when the doping concentration is further increases. As the doping concentration of the AZO layer increases, the resistance of the AZO layer decreases, which leads to an increase in the dark current.

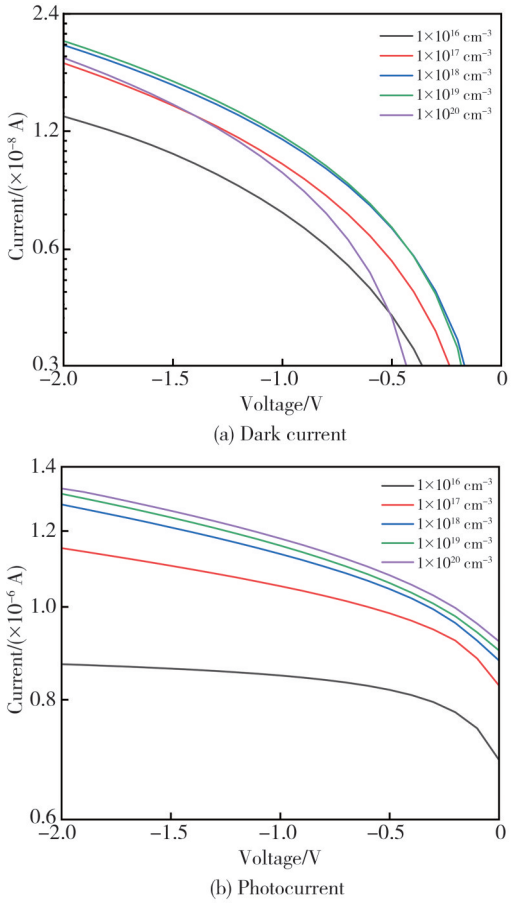

Fig. 9 *I*-*V* characteristics of AZO layer at different doping concentrations

Fig.10 shows the electric field distribution of the AZO layer at different doping concentrations. It can be seen that when the AZO doping concentration reaches 1×10^{20} cm^{-3}, the electric field at the ZnO-AZO interface increases significantly, this enhanced field facilitates the collection of thermally excited carriers, resulting in suppressed dark current. As the doping concentration of the AZO layer increases, the electric field intensity at the ZnO-AZO interface increases. This electric field prevents photogenerated holes from approaching the ZnO-AZO interface and reduces interfacial recombination, thus increasing the collection efficiency of photogenerated carriers[21], which leads to an increase in photocurrent. When the AZO doping concentration reaches 1×10^{20} cm^{-3}, the width of the undepleted region increases, which will lead to a decrease in the photogenerated carrier collection rate, so the photocurrent decreases.

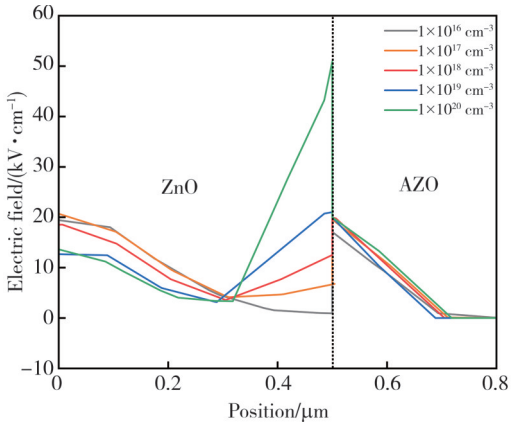

Fig. 10 Electric field distribution of AZO layer at different doping concentrations

Fig. 11 shows the responsivity of the AZO layer at different doping concentrations. It can be seen that the responsivity of the device to UV light is gradually enhanced with the increase of doping concentration, but the peak responsivity to UV light decreases at high doping concentration.

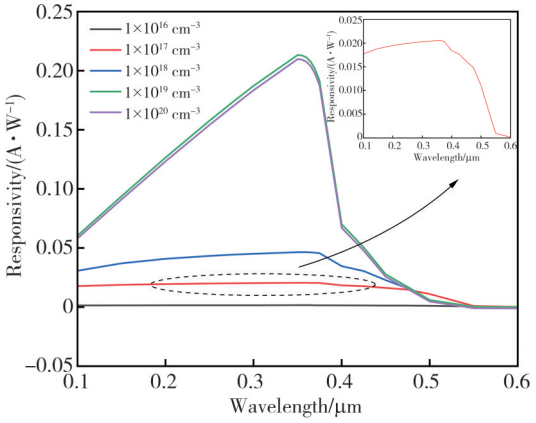

Fig. 11 Responsivity of AZO layer at different doping concentrations

The responsivity of the device is optimal when the doping concentration is 1×10^{19} cm^{-3}. In addition, the data reveal that for low doping concentrations, the responsivity of the device is weak and does not show high sensitivity to UV light, i.e., when the wavelength of the light beyond 400 nm, the responsivity of the device decreases slowly but not significantly. When the doping concentration reaches 1×10^{19} cm^{-3}, the device exhibits a sharp decline in

responsivity for wavelengths beyond 400 nm, indicating high UV sensitivity with effective visible-light suppression. In summary, the optimal doping concentration for the AZO layer is 1×10^{19} cm^{-3}.

2.4 Effect of ZnO layer doping concentration on device performance

The experimentally prepared ZnO films usually behave as n-type semiconductors due to intrinsic defects (oxygen vacancy and interstitial zinc) [22]. To investigate the influence of ZnO doping concentration on device performance, we characterized weakly n-type ZnO thin films with controlled doping concentrations ranging from 1×10^{14} cm^{-3} to 1×10^{17} cm^{-3}, and analyzed the resulting variations in photocurrent, dark current, electric field distribution, as well as responsivity.

Fig. 12 shows the *I-V* characteristics of ZnO layer at different doping concentrations.

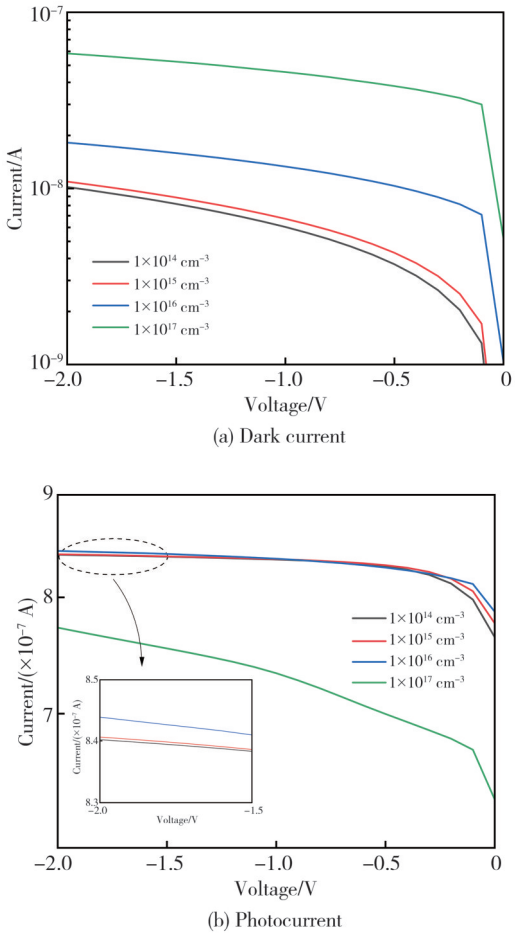

Fig. 12 *I-V* characteristics of ZnO layer at different doping concentrations

Fig. 12(a) shows the dark current of ZnO layer under different doping concentrations. With the increase of doping concentration, the dark current increases gradually. When the doping concentration reaches 1×10^{16} cm^{-3} and above, the dark current increases significantly. Fig. 12(b) presents the photocurrent of ZnO layer under different doping concentrations. The photocurrent shows a gradual increase across lower doping concentrations (1×10^{14}—1×10^{16} cm^{-3}), peaking at 1×10^{16} cm^{-3}. However, further increasing the concentration to 1×10^{17} cm^{-3} leads to a significant photocurrent reduction.

This behavior can be explained by the electric field distribution shown in Fig. 13. At moderate doping concentrations (1×10^{14}—1×10^{16} cm^{-3}), the depletion region width shows negligible narrowing. In this range, the increased free carrier concentration with doping enhances both dark current and photocurrent. However, when the doping concentration reaches 1×10^{17} cm^{-3}, a significant narrowing of the depletion region occurs. This contraction increases the carrier diffusion length, thereby enhancing recombination rate. Consequently, this leads to elevated dark current while reducing photocurrent.

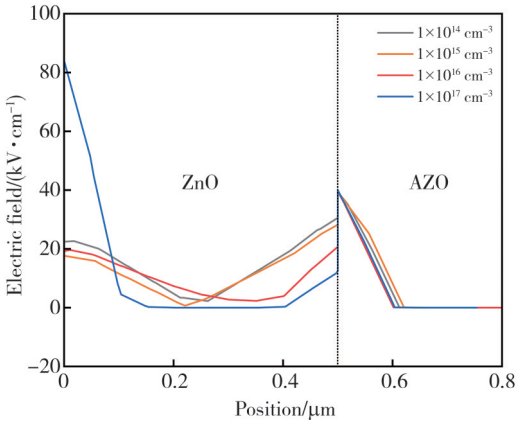

Fig. 13 Electric field distribution of ZnO layer at different doping concentrations

Fig. 14 presents the responsivity of the ZnO layer at different doping concentrations.

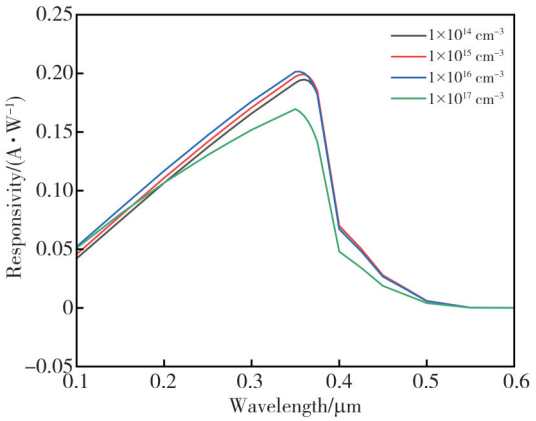

Fig. 14 Responsivity of ZnO layer at different doping concentrations

The device demonstrates a gradual responsivity improvement as the doping concentration increases from 1×10^{14} cm^{-3} to 1×10^{16} cm^{-3}, while maintaining excellent

UV-band response (<400 nm). However, further increasing the doping concentration to 1×10^{17} cm^{-3} leads to significant reduction of responsivity. In summary, the optimum doping concentration for the ZnO layer is 1×10^{16} cm^{-3}.

3 Conclusions

In this study, we constructed and simulated Ag/ZnO/AZO/Al photodetectors using Silvaco TCAD to investigate the effects of AZO layer thickness, ZnO layer thickness, AZO doping concentration, and ZnO doping concentration on device performance. The simulation results demonstrate that when the thickness of AZO layer is 0.8—1.2 μm, the photocurrent enhances from 1.07×10^{-6} A to 1.39×10^{-6} A, but the dark current increases from 1.02×10^{-8} A to 1.37×10^{-8} A synchronously, and the responsivity reaches 0.198 $A\cdot W^{-1}$ at the thickness of AZO equalling 1.2 μm. When the thickness of ZnO layer is 0.5—0.8 μm, the dark current decreases from 1.21×10^{-8} A to 1.11×10^{-8} A, and meanwhile, the photocurrent increases from 1.24×10^{-6} A to 1.42×10^{-6} A, and the responsivity reaches 0.21 $A\cdot W^{-1}$ at a ZnO thickness of 0.5 μm. When the AZO layer doping concentration is 1×10^{20} cm^{-3}, the dark current decreases to 1.11×10^{-8} A while the photocurrent reaches 1.33×10^{-6} A. Notably, the responsivity reaches 0.195 $A\cdot W^{-1}$ at an AZO layer doping concentration of 1×10^{19} cm^{-3}. When the ZnO layer doping concentration is 1×10^{15} cm^{-3}, the dark current is 1.1×10^{-8} A, the photocurrent reaches 8.41×10^{-6} A, and the responsivity reaches 0.202 $A\cdot W^{-1}$ when the ZnO layer doping concentration is 1×10^{16} cm^{-3}.

In this study, the Ag/ZnO/AZO/Al UV photodetectors are further investigated and tuned to provide theoretical guidance for the experimental preparation of ZnO/Ag Schottky photodetectors with AZO buffer layer on glass substrate.

Acknowledgement

This work was supported by Natural Science Foundation of Gansu Province (No. 23JRRA844).

Declaration of conflicting interests

The authors have no conflict of interests related to this publication.

References

[1] NASIRI N, BO R H, WANG F, et al. Ultraporous electron-depleted ZnO nanoparticle networks for highly sensitive portable visible-blind UV photodetectors. Advanced Materials, 2015, 27(29): 4336-4343.

[2] ALAIE Z, MOHAMMAD NEJAD S, YOUSEFI M H. Recent advances in ultraviolet photodetectors. Materials Science in Semiconductor Processing, 2015, 29: 16-55.

[3] OUYANG B S, ZHANG K W, YANG Y. Self-powered UV photodetector array based on P3HT/ZnO nanowire array heterojunction. Advanced Materials Technologies, 2017, 2(12): 1700208.

[4] SHARMA S, PERIASAMY C. Simulation study and performance analysis of n-ZnO/p-Si heterojunction photodetector. Journal of Electron Devices, 2014, 19: 1633-1636.

[5] VARMA T, PERIASAMY C, BOOLCHANDANI D. Performance analyses of Schottky diodes with Au/Pd contacts on n-ZnO thin films as UV detectors. Superlattices and Microstructures, 2017, 112: 151-163.

[6] DAS M, SARMAH S, BARMAN D, et al. Distinct band UV–visible photo sensing property of ZnO-Porous silicon (PS): p-Si hybrid MSM heterostructure. Materials Science in Semiconductor Processing, 2020, 118: 105188.

[7] ISMAIL R A, AL-SAMARAI A E, MOHAMMED W M. Preparation of n-ZnO/p-Si heterojunction photodetector *via* rapid thermal oxidation technique: effect of oxidation time. Applied Physics A, 2018, 124(8): 527.

[8] LIU Z, CHENG B W. Research progresses of Si-based Ge PIN photodetectors. Semiconductor Optoelectronics, 2022, 43(2): 261-266.

[9] LI H D, JIANG D Y, ZHAO M. High ultraviolet gain in Ga_2O_3/ZnO heterojunction photodetector based on MSM structure. Journal of Alloys and Compounds, 2024, 1005: 176217.

[10] JANARDHANAM V, JYOTHI I, ZUMUUKHOROL M, et al. High gain GaN ultraviolet Schottky photodetector with Al-doped ZnO interlayer. Surfaces and Interfaces, 2021, 27: 101405.

[11] SINGH S. Simulation, fabrication, and characterization of Al-doped ZnO-based ultraviolet photodetectors. Journal of Electronic Materials, 2016, 45(1): 535-540.

[12] AL-KHALLI N, ABOUD M, DEBBAR N. Theoretical study and design of n-ZnO/p-Si heterojunction MSM photodiode for optimized performance. Optics & Laser Technology, 2021, 133: 106564.

[13] AYDOĞAN Ş, GRILLI M L, YILMAZ M, et al. A facile growth of spray based ZnO films and device performance investigation for Schottky diodes: Determination of interface state density distribution. Journal of Alloys and Compounds, 2017, 708: 55-66.

[14] ZHANG C Z, HU T, WANG Z X, et al. Influence of AZO buffer layer on characteristics of ZnO film on glass substrates for Schottky UV photodetector applications. Optical Materials, 2024, 156: 115889.

[15] BANSAL S. Simulation and optimization of Pt/ZnO Schottky UV photodetector with Al ohmic contact//2024 3rd International Conference for Innovation in Technology, March

1-3, 2024, Bangalore, India. New York: IEEE, 2024: 1-6.
[16] YOUSEFIZAD M, GOLSHAN BAFGHI Z, SHAHRIYARI A, et al. Advancements in photovoltaic efficiency: The role of fluorine-doped CZTS in homojunction solar cells. Heliyon, 2025, 11(3): e42300.
[17] MA Y H, ZHANG W Q, CHEN C P, et al. First-principles study on electronic structure and photoelectric properties of Li-doped α-Bi_2O_3. Journal of North University of China (Natural Science Edition), 2023, 44(5): 503-509.
[18] BANSAL S, RAJPOOT A K, CHAMUNDESWARI G, et al. Pt/ZnO and Pt/few-layer graphene/ZnO Schottky devices with Al ohmic contacts using Atlas simulation and machine learning. Journal of Science: Advanced Materials and Devices, 2024, 9(4): 100798.
[19] NOVÁK P, OČENÁŠEK J, KOZÁK T, et al. Identification of electrical properties in individual thickness layers in aluminium-doped zinc oxide films sputtered at 100 ℃. Thin Solid Films, 2018, 660: 471-476.
[20] ZHANG C Z, CHEN Y G, ZHOU Q H. Method for improving properties of ZnO thin films prepared on the glass substrate. Semiconductor Technology, 2019, 44(6): 454-458.
[21] LI Y N, NIE S X, HUANG L L, et al. Paper based self-powered UV photodiode: Enhancing photo-response with AZO back-field layer. Ceramics International, 2023, 49(3): 4831-4838.
[22] YE Z Z, WANG F Z, CHEN F, et al. Wide band gap semiconductor optoelectronic materials and their applications. Acta Optica Sinica, 2022, 42(17): 1716001.

Ag/ZnO/AZO/Al光电探测器的模拟及分析

张彩珍*, 胡　彤, 方亨通, 沈玲琴

兰州交通大学 电子与信息工程学院, 甘肃 兰州 730070

摘　要： 在玻璃衬底上引入铝掺杂氧化锌(Aluminum-doped zinc oxide, AZO)缓冲层可以改善Ag/ZnO肖特基(Schottky)光电探测器的性能。为进一步研究AZO缓冲层及ZnO有源层与Ag/ZnO/AZO/Al光电探测器性能的关系, 基于Silvaco TCAD仿真平台构建了Ag/ZnO/AZO/Al光电探测器, 并研究了AZO层厚度、ZnO层厚度、AZO层掺杂浓度以及ZnO层掺杂浓度对器件性能的影响。仿真结果表明, 当AZO层厚度为0.8～1.2 μm, ZnO层厚度为0.5～0.8 μm, AZO掺杂浓度为1×10^{19} cm^{-3}, ZnO掺杂浓度为1×10^{16} cm^{-3}时, 器件性能较好。提高AZO缓冲层的掺杂浓度可增强ZnO-AZO界面处的电场强度, 从而有效阻止光生空穴接近ZnO-AZO界面以减少界面复合; 而适中的ZnO层厚度与掺杂浓度能够优化空间电荷区宽度和载流子收集效率。器件性能达到最佳时的暗电流为1.1×10^{-8} A, 光电流为8.41×10^{-6} A, 响应度达0.21 A·W^{-1}。本研究有效减小了实验次数、节约了试验成本, 为制备低成本、高性能ZnO光电探测器提供了有益的参考。

关键词： 铝掺杂氧化锌; 氧化锌; 肖特基; 紫外光电探测器; 电场分布; 暗电流

引用格式： ZHANG Caizhen, HU Tong, FANG Hengtong, et al. Simulation and analysis of Ag/ZnO/AZO/Al photodetector. Journal of Measurement Science and Instrumentation, 2026, 17(1): 133-140. DOI: 10.62756/jmsi.1674-8042.2026011